Carbon doped TiO_2 and carbon, tungsten co-doped TiO_2 through sol-gel processes in the presence of melamine borate: reflections through photocatalysis

Elaine M. Neville[a], Michael J. Mattle[b], David Loughrey[c], Bashyam Rajesh[b], Mahfujur Rahman[c], J.M. Don MacElroy[c], James A. Sullivan[a] and K. Ravindranathan Thampi[b],[c]†**

[a] SFI Strategic Research Cluster in Solar Energy Conversion, UCD School of Chemistry and Chemical Biology, Belfield, Dublin 4, Ireland.

[b] Laboratory of Photonics and Interfaces, ISIC, École Polytechnique Fédérale de Lausanne, CH-1015, Lausanne, Switzerland.

[c] SFI Strategic Research Cluster in Solar Energy Conversion, UCD School of Chemical and Bioprocess Engineering, Belfield, Dublin 4, Ireland.

Corresponding authors: *James.Sullivan@ucd.ie *Ravindranathan.Thampi@ucd.ie

† Current address, UCD School of Chemical and Bioprocess Engineering, Belfield, Dublin 4, Ireland.

KEYWORDS: TiO_2, photocatalysis, band gap engineering, solar energy

ABSTRACT

A series of C-doped, W-doped and C,W co-doped TiO_2 samples have been prepared using modified sol-gel techniques. Reproducible inexpensive C-doping arises from the presence of melamine borate in a sol-gel mixture while W-doping is from the addition of tungstic acid to the sol. The materials have been characterised using elemental analysis, N_2 physisorption (BET), Thermogravimetric analysis (TGA), X-Ray diffraction (XRD), Raman, X-ray photoelectron (XPS) and UV-Vis spectroscopies, and photocatalytic activity measurements.

Doping C and W independently results in an increased absorbance in the visible region of the spectrum with a synergistic effect in increased absorbance when both elements are co-doped. The increased visible light absorbance of the W-doped or co-doped materials is not reflected in photocatalytic activity. Visible light induced photocatalytic activity of C-doped material was superior to that of an un-doped catalyst, paving the way for its application under only visible light irradiation conditions. A significant fraction of the spectral red-shift commonly observed with doped catalysts might be due to the formation of colour centres as a result of defects associated with oxygen vacancies, and bandgap related narrowing or intragap localization of dopant levels are not the only factors responsible for enhanced visible light absorption in doped photocatalysts. Furthermore, bandgap narrowing through increases in the energy of the valance band may actually decrease photo-oxidation activity through a curtailment of one route of oxidation.

1. INTRODUCTION.

The initial step of all photocatalytic processes promoted by semiconductor materials involves the absorption of a photon of energy $\geq E_g$ (bandgap), which promotes an electron from its valence band (VB) to the conduction band (CB). This generates an electron (e^-) in the CB and leaves behind a hole (h^+) in the VB [1, 2]. The former can act as a reductant and the latter as an oxidant in the different photocatalytic and photosynthetic processes being considered, *e.g.* water splitting to hydrogen and oxygen [3, 4], pollutant oxidation [5, 6] or aqueous phase reforming of organic compounds [7, 8]. TiO_2 is the ubiquitous photocatalyst due to its low cost, bio-compatibility, its chemical and biochemical stability and its interesting photocatalytic activity [9, 10].

One of the major limitations associated with the use of TiO_2 for solar driven photocatalysis is that the E_g of pure anatase TiO_2 (3.2 eV) is too large for visible light to promote an electron from the valance band to the conduction band [4]. In effect, this limits the use of TiO_2 as a photocatalyst to only harvesting the UV component of the terrestrially available sunlight. Since the majority of solar radiation incident on the surface of the planet has insufficient energy to initiate TiO_2 photocatalysis, the efficiency of such solar-driven processes is significantly compromised.

One way to counter this limitation and shift absorbance into the visible region of the solar spectrum is to alter the bandgap of TiO_2 through selective doping. A wide variety of dopants

have been studied including both metallic and non-metallic elements [11-24]. Doping of TiO_2 with non-metals (specifically C and N) has attracted significant attention [11, 12, 14, 15, 17-19, 21, 23-25]. Co-doping of C and N has also been investigated [12]. There are several reports combining the two approaches *i.e.* metal and non-metal ions co-doped TiO_2 photocatalysts, *e.g.* co-doping with nitrogen and various metal ions, has been studied [26, 27], and to a lesser extent carbon and tungsten co-doping [28].

In this work we have prepared and characterised a series of carbon-doped, tungsten doped and carbon – tungsten co-doped TiO_2 catalysts. The preparations have involved sol-gel procedures using $TiCl_4$ and tungstic acid precursors in which the carbon source has been a melamine borate salt added to the preparation mixture. Melamine salts have been chosen as the source of the carbon dopant due to the fact that their deep oxidation requires relatively high temperatures. Thus, following the formation of TiO_2 from calcination of the sol-gel derived precursor, dopant amounts of carbon can remain within the lattice. The formation of the materials during calcination has been studied using TGA with residual gas analysis while the textural properties of the final powders have been characterized using N_2 physisorption. Their morphologies have been confirmed using XRD and Raman spectroscopy. The carbon levels within the samples has been analysed using elemental analysis while the nature of the carbon doping (near the surfaces of the TiO_2 particles) has been evaluated using XPS. The electronic properties of the materials have been monitored using Diffuse Reflectance UV–visible spectroscopy and their activities have been probed using a model photo-catalytic reaction and the results interpreted based on different reactions involving the photo-generated electrons and holes.

2. EXPERIMENTAL

Preparation of TiO_2, C-doped TiO_2 and W, C-co-doped TiO_2: TiO_2 and doped TiO_2 materials were formed using hydrolysis of $TiCl_4$ (followed by condensation) to form the $X_3Ti\text{-}O\text{-}TiX_3$ lattices (where X represents OH or $\text{-}O\text{-}TiX_3$ groups). In the case of C-doped catalysts the carbon was derived from melamine borate which was added to the mixture prior to hydrolysis. Tungsten doping was introduced through the addition of tungstic acid to the mixture.

In a typical synthesis of C-doped TiO_2 3.4 g of melamine borate (Budenheim, Germany) was dissolved in 0.5 L deionised water under constant stirring at room temperature. After 24 h, the solution was filtered through Whatman Grade 1 filter paper. 11 mL $TiCl_4$ (≥99.0% (AT), Fluka) was slowly dissolved in 1.5 L of deionised water at 2 – 4 ºC. To this solution, various aliquots (3.5 mL, 7 mL and 14 mL) of melamine borate solution were added and stirred for 30 minutes. Nominally (assuming all carbon added remains in the final prepared material), this represents C doping at levels of 1 %, 2 % and 4 % respectively (see below). A 2.5 M solution of ammonium hydroxide (made through dilution of a 26 % solution, Riedel-de Haen, Germany) was added drop-wise until pH 5 was reached. This resulted in precipitation of the TiO_2 precursor from the solution. The precipitate obtained was allowed to settle overnight before being filtered through Whatman Grade 1 filter paper and washed repeatedly with warm de-ionised water (to eliminate Cl^- from the solid). The removal of Cl^- was confirmed using a standard $AgNO_3$ precipitation test. The solid was then dried at 80 ºC overnight. The resultant material was ground into fine powder and calcined at 400 °C for various lengths of time (1 h, 3 h, 15 h, etc.).

The nominal levels of doped C mentioned above assume that all the carbon in the melamine borate remains in the material following calcination. Obviously this is not the case as significant portions are removed during the calcination step or remain in the supernatant fluid as the pre-catalyst material crystallises from solution. The actual levels of C remaining within or upon the materials were determined using microanalysis. The final products were yellow powders.

Similarly, a series of W–doped catalysts was prepared using different concentrations of tungstic acid (99 %, Aldrich) within the precipitating mixture [16]. The co-doped TiO_2 materials were synthesized following the addition of both tungstic acid and melamine borate to the mixture. 1 %, 5 % and 10 % W-TiO_2 (mass %) were produced. The W containing material was dried at 80 °C overnight and then ground to a fine powder before being calcined for 15 hours at 400 °C. The materials produced were again yellow in colour.

Analysis of the calcination process: A Hiden analytical HPR20-QIC atmospheric gas analysis system coupled to a thermogravimetric analyzer (TA Instruments, TGA 500) was used in the analysis of the material calcination steps. The dried pre-catalysts were held in a flow of air (100 mL min^{-1}) and while the temperature was raised using a linear rate of increase (20 °C min^{-1}) the exit gas was continuously analysed by mass spectrometry. Profiles of the evolved CO_2, NO and H_2O were recorded as a function of temperature. Typically, an aliquot of 50 mg of the dried precursor was loaded onto a balance within the TGA. The sample was held in a flow of air at room temperature for 1 h. The temperature was then ramped at a rate of 20 °C min^{-1} to 400 °C

and held at this temperature for 1 h (to mimic the calcination process) or ramped 20 °C min^{-1} up to 1000 °C (to analyse the material following calcination). The temperature of removal and the extent of removal (through combustion) of the various carbon-containing species present in the materials both during and following calcination were monitored in this way.

Catalyst characterisations: Diffuse Reflectance UV-vis spectroscopy (DRS) was carried out using an Analytik Jena Specord 210 spectrometer equipped with an integrating sphere attachment for measurement of spectra from powder samples. Band gaps were estimated by drawing a tangent to the high-energy feature and approximating a bandgap energy from the wavelength at which the tangent intercepts a line with an absorbance value of zero. Raman spectra were obtained using a SENTERRA Dispersive Raman Microscope (Bruker Optics) with a 785 nm laser. Powder XRD patterns were collected using a Siemens D500 Kristalloflex using Cu Kα radiation. N_2 physisorption isotherms were collected on a Quantachrome Nova 2000e. X-ray Photoelectron Spectroscopy (XPS) was carried out with a Kratos AXIS 165 spectrometer using a monochromatic X-ray source (Al Kα 1486.58 eV). Elemental analysis was performed using various techniques: C, H, N analysis was carried out with a CE-440 elemental analyser (Exeter Analytical, Inc.) using thermal conductivity detection for measurement following combustion and reduction. Cl^- analysis was performed using Oxygen flask combustion followed by filtration. W analysis and further Cl^- analysis was carried out using EDX with a FEI Quanta 3D FEG DualBeam (FEI Ltd, Hillsboro, USA) SEM coupled to an EDAX EDX APOLLO XV Silicon Drift Detector.

Photocatalytic activity measurements: Photocatalytic activity of the materials was tested by investigating the initial photocatalytic degradation of 4-chlorophenol solutions. 80 mg of photocatalyst powder was dispersed in 40 mL of a 0.5 mM solution of 4-chlorophenol. The mixture was sonicated for 15 min before being purged with air for 5 min. Samples were stirred in the dark for 30 min in order to reach an adsorption – desorption equilibrium. Irradiation was carried out in an Atlas Suntest CPS (AM1.5 G) solar simulator unit with (when required) a UV filter film ($\lambda > 410$ nm). Samples were extracted hourly for 5 hours and the degradation (complete mineralisation) of 4-chlorophenol was monitored using Total Organic Carbon (TOC) analysis (Shimadzu TOC V-CPH).

3. RESULTS AND DISCUSSION

In most doped photocatalyst studies, there is an uncertainty as to whether the dopant is truly in a doped state and, when truly doped, whether it resides preferentially in the TiO_2 bulk or on the surface. Depending on these variations the photocatalytic reaction mechanisms would show changes. Therefore, the levels of dopants were analysed by both elemental analysis and XPS, in attempts to differentiate whether all the carbon found in the sample is of a doped nature and whether they are selectively enriched on the surface with respect to the bulk. The XPS measurements (see later), besides providing solely the surface concentration, is also able to give an insight into the nature of the carbon species located on the surface.

In all cases (for doped and undoped samples) elemental analysis shows that the total levels of carbon in the samples is between 0.01 and 0.03%. There is no relationship between the amount of melamine salt used in the preparation and the eventual measured concentration of C in the material, *i.e.* C-TiO_2 materials showed similar levels of carbon content irrespective of the levels of melamine borate added initially to the preparation mixture and similar levels of carbon were noted on samples that nominally were un-doped. This suggests that the concentrations of surface carbon, including carbonate on the materials, *e.g.* arising from adsorption of CO_2, are significantly higher than the levels of carbon dopants incorporated in the bulk. However, as noted by XPS (see later) the nature and dispersion of carbon on the doped samples differs from that in the un-doped samples. Table 1 shows the measured levels of W in the W-doped samples as well as the absorption onsets and calculated bandgaps of the materials. The tungsten and co-doped samples showed a trend for slightly reduced levels of carbon (0.01 – 0.02 mass %). This may partially be due to the incorporation of the heavier W^{6+} ion influencing the relative mass % values.

Table 1. Measured [C] and [W], absorption onsets and bandgap estimates for the doped TiO_2 materials. The indicated times refer to the length of the calcination step for the relevant materials.

Theoretical % doping	% C (Elemental analysis)	% W (EDX)	Absorption onset (nm)	Bandgap (eV)
P25 TiO_2	0.03	-	410	3.02
1 % C-TiO_2, 1 h	0.03	-	425	2.92
2 % C-TiO_2, 1 h	0.02	-	425	2.92
4 % C-TiO_2, 1 h	0.03	-	430	2.88

1 % C-TiO_2, 3 h	0.02	-	430	2.88
2 % C-TiO_2, 3 h	0.02	-	430	2.88
4 % C-TiO_2, 3 h	0.03	-	430	2.88
1 % W-TiO_2	0.01	1.40	433	2.86
5 % W-TiO_2	0.02	5.79	438	2.83
10 % W-TiO_2	0.01	9.80	442	2.80
1 % C, 1% W-TiO_2	0.02	1.21	438	2.83
1 % C, 5% W-TiO_2	0.01	5.15	450	2.76
1 % C, 10% W-TiO_2	0.02	7.11	465	2.67
2 % C, 1% W-TiO_2	0.01	1.27	442	2.81
2 % C, 5% W-TiO_2	0.01	4.19	460	2.70
2 % C, 10% W-TiO_2	0.01	10.24	470	2.64
4 % C, 1% W-TiO_2	0.01	1.23	435	2.85
4 % C, 5% W-TiO_2	0.02	3.83	465	2.67
4 % C, 10% W-TiO_2	0.02	7.10	480	2.58

Thermogravimetric-Mass spectrometry (TGA-MS) analysis was carried out on the catalyst precursor to mimic the calcination of the material. The precipitate from a C-TiO_2 preparation (with a nominal 4% C-doping) was heated up to 400 °C in air. These TGA and evolved gas profiles (Figure 1 (a) and (b)) show a range of oxidation events with the release of CO_2, H_2O and NO (from the combustion of melamine in the pre-catalyst) peaking at a temperature of ~260 °C. This confirms that significant amounts of melamine are still present in the precipitated material and large amounts of these are removed from the catalyst during calcination.

Figure 1(c) shows the results of a TGA carried out on a catalyst which had previously been calcined at 400 °C for 1 h. An approximate 2 % weight change is observed at temperatures lower than 400 °C. This presumably is due to the removal of adsorbed or condensed species on the surface. A further weight change is observed at higher temperature (600 – 800 °C) which may be attributable to removal of the carbon dopant and / or oxygen loss resulting in the formation of Magnéli phase TiO_{2-x} sub-oxides [29]. No CO_2 was observed in the exit gas concurrent with this peak (although any CO_2 formed from the combustion of the small amounts of dopants would be difficult to detect under these conditions). Following the thermal treatment the catalyst acquired a light grey colour.

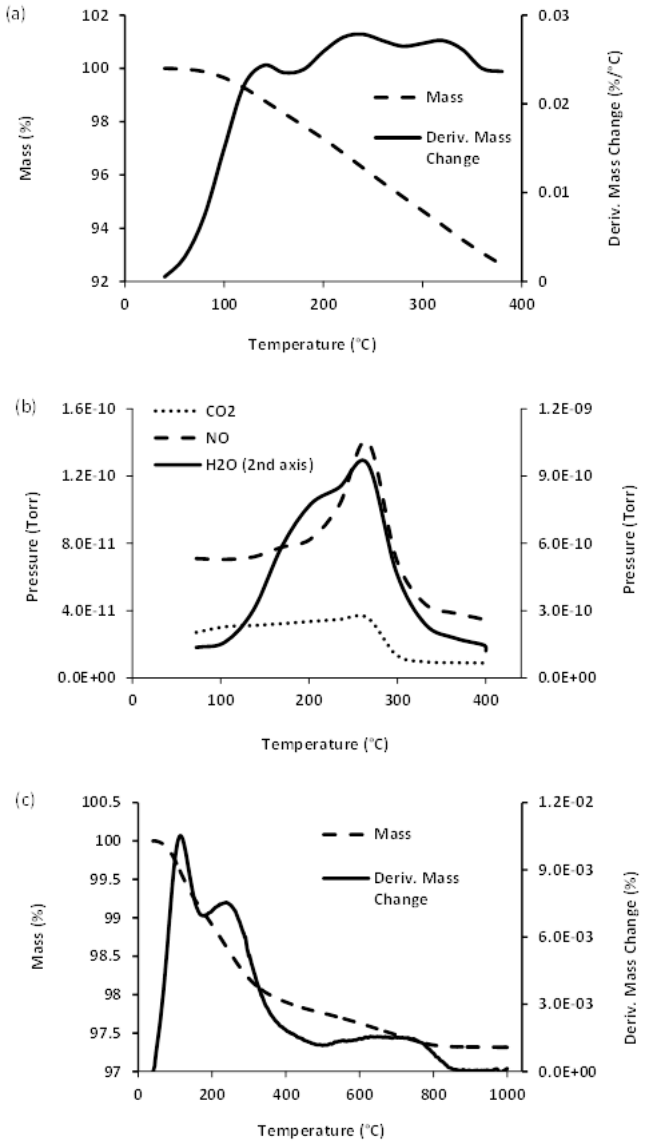

Figure 1 (a) TGA and DTGA profiles measured during the calcination of the pre-catalyst to 400 °C, (b) evolved gas analysis from the same experiment and (c) TGA and DTGA profiles of an already calcined sample of C-TiO_2. All catalysts are with a nominal loading of 4% C, based on the amount of melamine borate added initially.

XRD patterns were obtained to determine the crystal phase of the photocatalysts. Figure 2 shows the XRD patterns of the C-doped TiO_2 materials series calcined at 400 °C for 1 h. The powder shows anatase phase peaks (JCPDS: No 21-1272). The nominally 4% Carbon TiO_2 also displays an additional peak at about 30 ° confirming trace levels of brookite formation (JCPDS: No 29-1360) [30]. After a 3 h calcination step this peak disappears (see Figure 2).

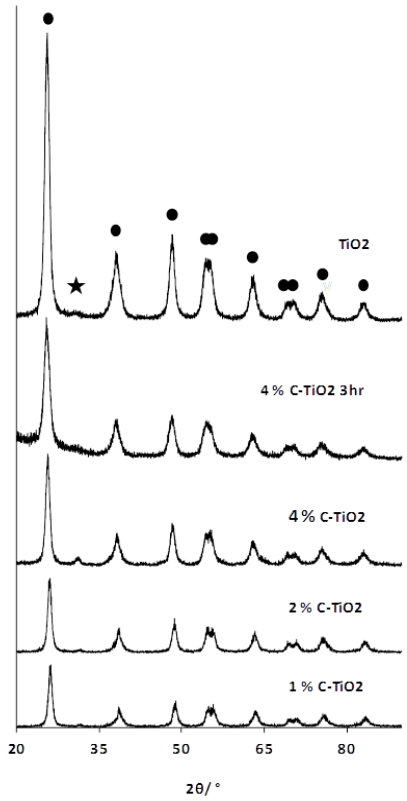

Figure 2. XRD patterns of C-doped TiO_2. Samples with nominal dopant levels of 1 %, 2 % and 4 % calcined at 400 °C for 1 h, and a sample with a nominal dopant level of 4 % calcined at 400 °C for 3 h (upper profile) (●) indicates anatase and (*) brookite phases.

XRD patterns of W-doped TiO_2 materials (with different levels of W incorporated) and the profiles collected from C, W co-doped materials are shown in Figure 3. In the case of the solely W-doped samples, some rutile peaks are also evident (note □). However, tungsten incorporation has been reported to retard the transition from anatase to rutile [31, 32] and our result seems to contradict this observation. Peaks relating to the rutile phase are however absent in the co-doped materials.

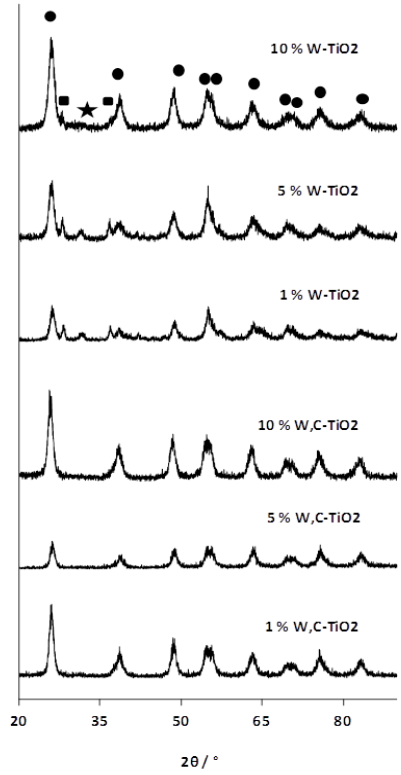

Figure 3. XRD profiles of W-doped TiO_2 samples with nominal loadings of 1 %, 5 % and 10 % W and C-W co-doped samples containing nominally 4 % C and 1 %, 5 % and 10 % W. (●) indicates anatase, while (■) indicates rutile and (*) indicates brookite phases.

Raman spectra (not shown) also confirm the presence of the anatase phase in all the samples, *i.e.* 6 Raman active modes were noted (A_{1g} (519 cm^{-1}), B_{1g} (399 and 519 cm^{-1}), and E_g (144, 197, and 639 cm^{-1})) – all consistent with the presence of the anatase phase. The W-TiO_2 materials also showed additional smaller Raman active modes at 232, 446, and 609 cm^{-1}, confirming the presence of the rutile phase.

The crystallite particle size, as calculated using the Scherrer equation [33] applied to the XRD peak (101) at 2θ = ~25 °, (with shape factor K = 0.94), and surface area of the various photocatalysts, as determined using BET, are summarised in table 2. As expected, an increase in calcination time of the C-TiO_2 materials from 1 h to 3 h resulted in an increase in crystalline particle size approximately from 6 to 10 nm due to greater sintering of the material.

Increasing the concentration of melamine used during preparation also slightly affected the crystalline particle size of the C-TiO_2 materials. Materials with nominally 4% C which had been calcined for 3 h had particle sizes of approx. 9 nm while those with lower nominal [C] were slightly larger, with particle sizes of approx. 10 nm. This may be due to dissimilar boundaries created by carbon doping [34] resulting in slower rates of crystal growth and hence smaller crystallite size when the heating is prolonged for a longer time.

Table 2. Crystalline particle size (estimated using the Scherrer Equation), BET surface areas, pore radii and volumes of representative samples of C-doped, W-doped and C, W co-doped TiO_2 materials.

Theoretical % doping	particle size (nm)	surface area (m^2g^{-1})	pore radius (Å)	pore volume (cc/g)
P25 TiO_2	13.8 (anatase)	58.0	36.3	0.09
1 % C-TiO_2, 1 h	6.3	141.1	53.0	1.40
2 % C-TiO_2, 1 h	6.5	149.2	50.5	1.60
4 % C-TiO_2, 1 h	6.4	148.2	50.5	1.80
1 % C-TiO_2, 3 h	10.3	105.0	36.4	0.33
2 % C-TiO_2, 3 h	10.1	127.0	36.4	0.38
4 % C-TiO_2, 3 h	9.4	123.1	47.2	0.37
1 % W-TiO_2	7.8	89.8	29.6	0.20
5 % W-TiO_2	6.7	99.2	18.6	0.17
10 % W-TiO2	5.9	123.1	18.5	0.20
1 % C, 1% W-TiO_2	8.2	104.9	36.5	0.29
1 % C, 5% W-TiO_2	7.8	109.8	36.6	0.26
1 % C, 10% W-TiO_2	8.3	141.0	36.6	0.37
2 % C, 1% W-TiO_2	9.5	106.5	47.0	0.34
2 % C, 5% W-TiO_2	9.5	136.8	36.4	0.33
2 % C, 10% W-TiO_2	7.7	137.1	29.7	0.30
4 % C, 1% W-TiO_2	9.3	104.5	47.4	0.30
4 % C, 5% W-TiO_2	8.0	125.5	36.8	0.29
4 % C, 10% W-TiO_2	7.4	152.1	36.5	0.32

The W-containing materials, despite having an increased calcination time of 15 h, did not show any further increase in crystallite size compared to C-doped materials. This may be due to W incorporation slowing crystal growth rates [16, 31, 32] which could be attributed to increased formation energies as evidenced by higher Madelung constants. Furthermore, an increase in nominal levels of W dopant from 1 to 10 % also resulted in a decrease in particle size from approximately 8 to 6 nm and an increase in surface area.

Particle size and surface area measurements of the co-doped materials, in general, showed little change with increased levels of melamine borate used in the preparation mixture, but did display a slight decrease in crystallite size upon increased incorporation of W dopant. Again, surface areas increased with decreased particle size.

Figure 4 shows the UV-Vis Diffuse Reflectance Spectra (DRS) for the prepared samples using the spectrum of Degussa P25 TiO_2 as a reference profile. The absorption onset of the doped materials (which are yellow) is pushed further towards the visible region compared to P25 (which is white). Absorption onsets were used to estimate the bandgaps of the various materials and these are reported in Table 1 using the equation $E_g = hc/\lambda$, where E_g is the band gap energy (J), h is Planck's constant, c is the velocity of light, and λ is the wavelength (m) of absorption onset [12].

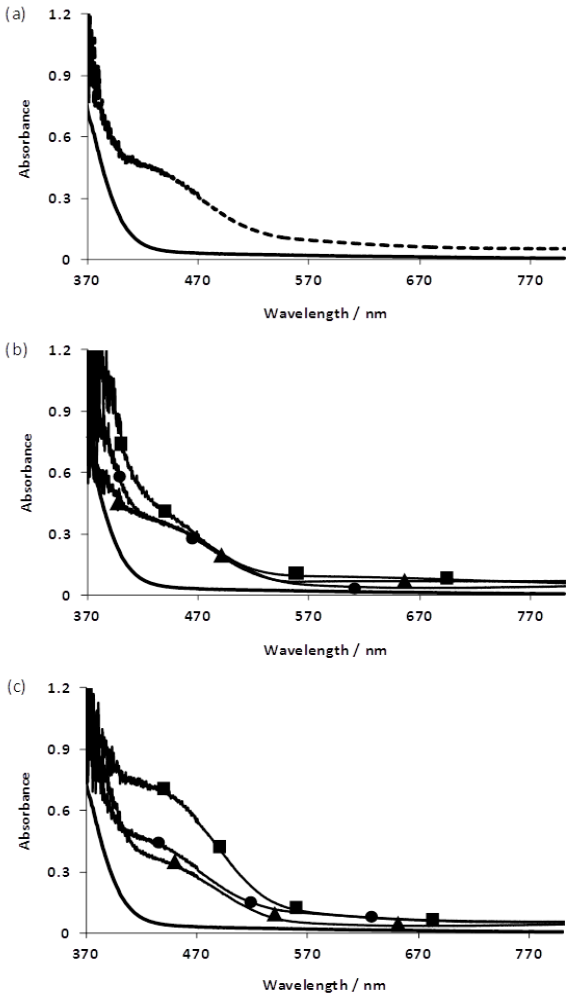

Figure 4. Diffuse Reflectance UV-Visible spectra of (a) TiO_2 (full line) and a C-doped TiO_2 sample nominally containing 4 % C (dashed line), (b) TiO_2 (full line) and W-doped TiO_2 containing 1% (●), 5% (■) and 10% (▲) W and (c) TiO_2 (full line), C-doped TiO_2 (nominally containing 4 % C) (●), W-doped TiO_2 containing 1% W (▲) and co-doped TiO_2 nominally containing 4 % C and 1% W (■).

It is clear that the presence of the carbon dopant (Figure 4(a)) increases absorbance towards the visible region. Increasing the nominal concentration of the dopant in the material (by increasing the concentration of melamine borate used during the preparation) had little effect on the position of the absorption onset or the calculated bandgap (see table 1).

Doping with W also increased the absorbance in the visible region (see Figure 4(b)) but in this case there seems to be an inverse relationship between the extent of W doping and the bandgap, *i.e.* the bandgap decreases as the [W] is increased. This relatively minor effect varies from a decrease of 0.07 eV in undoped catalysts when [W] doping is changed from 1% to 10% to a decrease of up to 0.27 eV for similar W doping levels in samples that nominally had 4% C.

The extents of the increases seen in visible light absorption are comparable when either W or C are used as dopants (compare Figure 4(a) and Figure 4(b)). Co-doping, as expected from recent theoretical calculations [35], increases further the fraction of visible light that is absorbed (see Figure 4(c)). This is reflected in the decreased calculated bandgaps (see table 1) and may be explained by an increase in the energy of the valance band upon doping with carbon and a decrease in the energy of the conduction band upon doping with tungsten [35].

XPS analysis was carried out in order to characterize the effect of doping and the chemical nature of the C, Ti, W and O atoms present at, or close to, the surface of the doped samples. The presence of new C 1s peaks was expected to directly confirm carbon doping, while shifts in the

Ti 2p and O 1s binding energies (which are reported to confirm lattice distortion [36]) were expected to indirectly confirm doping.

The C 1s regions of the XPS profiles were studied for both the doped and un-doped P25 TiO_2. Initially three peaks were seen at binding energies of 284.8, 286.2 and 288.7 eV. The peak at 284.8 eV is an instrumental artefact related to elemental adventitious carbon [37] present in all XPS measurements. The peaks at 286.2 and 288.7 eV have previously been related in the literature to interstitial carbonate dopants as well as oxidised carbon species adsorbed on the surface of the material [18, 34, 38-40]. These peaks were found to be present in both the doped and un-doped samples and must simply be related to carbon contaminants on the surface of the samples. We therefore cannot derive any conclusions on the existence of doping from the binding energies of the electrons related to these C 1s core levels.

XPS analysis of the C-doped and un-doped samples was then carried out after sputtering samples for 8 min with low energy Ar ions (2 keV) followed directly by sputtering for 5 min with high energy Ar ions (4 keV). The purpose of this treatment was to remove adsorbed carbon contaminants by etching away the top surface layers of the material. The peak at 284.8 eV, *i.e.* the instrumental artefact (see above) remained in the spectra of all samples. However, the intensity of the C 1s peaks at 286.2 and 288.7 eV (relating to carbonate species) decreased continually upon sputtering (Figure 5). A new peak at 282.1 eV was revealed in the carbon doped sample after sputtering. This peak is only observed after removal of the masking

carbonate species (present in the top layer of the sample) and has been related to Ti-C, or carbon substitutionally doped in the place of oxygen in the TiO_2 lattice [41-44] in literature.

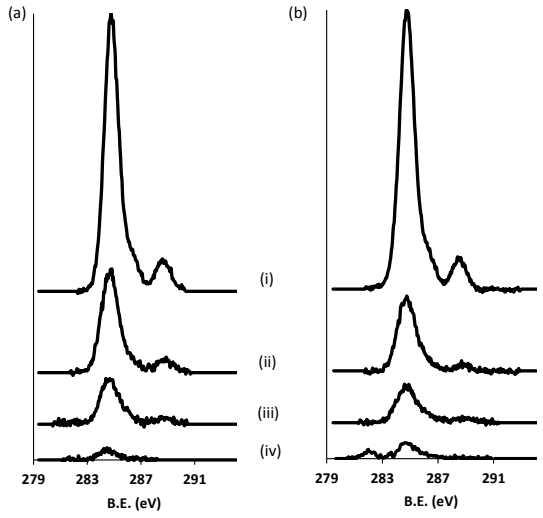

Figure 5. XPS C 1s peaks of (a) TiO_2 and (b) C-doped TiO_2 (with a nominal loading of 4 %) (i) before sputtering, (ii) after sputtering with 2 keV Ar^+ ions for 2 min, (iii) after sputtering with 2 keV Ar^+ ions for 8 min and (iv) after sputtering with 2 keV Ar^+ ions for 8 min and 4 keV Ar^+ ions for 5 min. Note the emergence of a new peak at 282 eV in the sample which had been doped with C.

The carbon dopant concentration, as measured using XPS, was determined from the intensity of the carbide C 1s peak at 282.1 eV. The un-doped TiO_2 (after sputtering for 8 min. with low energy Ar ions (2 keV)) contained 0 atom % carbon while the doped TiO_2 material studied contained 0.5 atom % carbon. Total surface carbon content including adventitious surface adsorbed elemental carbon and carbonate species (before sputtering) as measured using XPS was

naturally higher again (25.6 atom % for the un-doped and 27 atom % for the C-doped material). This measured carbon levels (0.5 atom % (or 0.225 mass %)) for the sputtered TiO_2 materials suggests that there is surface enrichment of carbon on these samples as the elemental analysis results showed only 0.03 mass % carbon in the entirety of this particular sample.

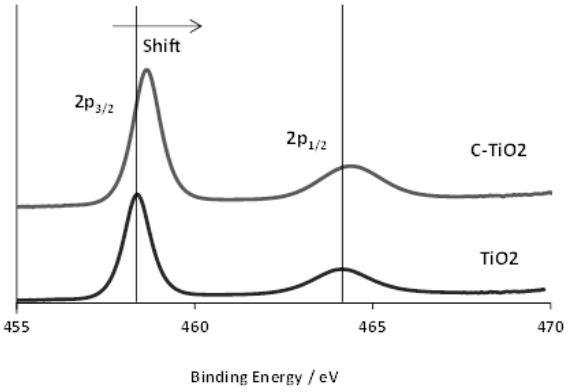

Figure 6. XPS Ti 2p peaks of TiO_2 and C-doped TiO_2 (with a nominal loading of 4 %). Note the increase in the Ti 2p binding energy upon C-doping.

Before sputtering, as was expected, two peaks were observed in the Ti 2p region relating to ejection of electrons from Ti $2p_{3/2}$ and Ti $2p_{1/2}$ levels. The Ti $2p_{3/2}$ binding energy for the un-doped TiO_2 sample was 458.3 eV. The Ti $2p_{3/2}$ binding energy for the C-doped TiO_2 samples was 458.6 eV, an increase of 0.3 eV. The Ti $2p_{1/2}$ binding energy for the un-doped P25 (Degussa) TiO_2 sample was 464.0 eV while the analogous peak for the C-doped sample was 464.4 eV, again an increase but this time of 0.4 eV. In both cases the binding energy increases upon C-doping (Figure 6). This may indicate lattice distortions.

There were also two peaks observed in the O 1s region relating to oxide and hydroxyl oxygen. The O 1s binding energies for the C-doped samples, when compared to the O 1s binding energies of un-doped P25 (Degussa), also displayed a slight shift. This was from 529.6 eV in the un-doped TiO_2 materials to 529.9 eV in the doped sample, and from 530.9 in the un-doped to 531.5 in the doped sample. Again, this may indicate lattice distortion upon doping.

The tungsten containing materials displayed two peaks in the W 4d region relating to ejection of electrons from W $4d_{5/2}$ and W $4d_{3/2}$ levels at 247.2 and 259.7 eV (see supporting information figure S1) and a peak at 36.6 eV due to electron ejection from the W 4f level These readings are consistent with literature reports on tungsten doped TiO_2 [27, 45].

Furthermore, the N 1s and B 1s regions of the XPS spectra were studied to investigate the possibility of N and B present as additional dopants from the melamine borate. Neither N 1s peaks (~ 400 eV) nor B 1s peaks (~190 eV) were observed (see supporting information figure S2 and S3 respectively). This shows (perhaps surprisingly), that, despite the high N content in melamine (and the NH_4OH used during the preparation), that little or no N was incorporated into the TiO_2 as a dopant. It is evident that during the solution processing and the subsequent washing, filtering and calcination steps, these elements are removed as side-products.

These results contrast somewhat with those in recent literature reports where Kisch *et al.* [46] investigated the nature of N-doped/modified TiO_2 formed from urea or melamine. They found that a key step in the formation N-doped/modified TiO_2 from this precursor was the TiO_2 catalysed formation of melamine, followed by various self-condensations to form a mixture of oligo-nuclear aromatic amines. This was followed by further condensation between the triazine amino groups of these molecules and surface hydroxyl species on TiO_2 to generate Ti-N bonds. These materials then showed activity in promotion of the photo-decomposition of formic acid under visible light irradiation. The authors suggest that neither nitridic species, nor NO_x species, nor TiO_2 defect states are responsible for this reactivity, but rather melamine condensation products acting as visible-light sensitizers.

The authors clearly show N-doping of their TiO_2 materials when using melamine as a dopant, in contrast to the results shown here (where only C-doping is observed). However there are several differences in the synthesis procedures used in the preparation of our materials and those of Kisch *et al.* [46]. Firstly, in [46] the levels of melamine used were significantly higher in their case (with catalyst:melamine ratios of 1:2) compared to our case where we would have a vast excess of TiO_2 precursor compared to organic material. Secondly, and more importantly, Kisch's materials were produced by grinding pre-formed TiO_2 with urea or melamine/melamine derivatives followed by calcination. The melamine (or melamine condensation products) are attached to the surface of the TiO_2 through condensation with surface hydroxyl groups. The materials prepared here are produced by introducing melamine into the pre-TiO_2 sol (*via* a melamine borate solution) before hydrolysis and condensation of the sol to form TiO_2. Any melamine not incorporated into the pre-TiO_2 lattice is removed *via* washing and filtration before

drying and calcination. There is no opportunity for high levels of the surface condensation reactions seen in [46].

Photocatalytic experiments were carried out to study whether the increased light absorption also resulted in an increased photocatalytic activity. The photocatalytic degradation of 4-chlorophenol in the presence of the photocatalysts under visible light (λ > 410nm) was investigated by determining the remaining levels of dissolved organic carbon-containing compounds at various time intervals following initiation of the reaction. Chlorophenols are ideal model compounds for characterizing the photocatalytic activity of pristine and doped TiO_2. Total organic carbon (TOC) measurements have previously shown that they undergo total mineralization by TiO_2 photocatalysts [47, 48].

Figure 7 shows the degradation versus time profiles for the photocatalytic oxidation of chlorophenol under visible light only (determined using TOC analysis). It is clear that carbon-doped TiO_2 material calcined for 1 h shows the highest photocatalytic ability, degrading approximately 71 % of the chlorophenol in 300 min. A carbon-doped TiO_2 sample which had been calcined for 3 hours was less effective, degrading about 63 % of the initial concentration of chlorophenol in the same time interval, despite this being a more crystalline material [49] and having a smaller band gap (see Table 1). The photocatalytic degradation process is reportedly heavily influenced by morphology, phase, chemical composition and particle size [50-53]. The smaller crystalline particle size and increased surface area of the material calcined only for 1 h appear to have enhanced the photocatalytic activity.

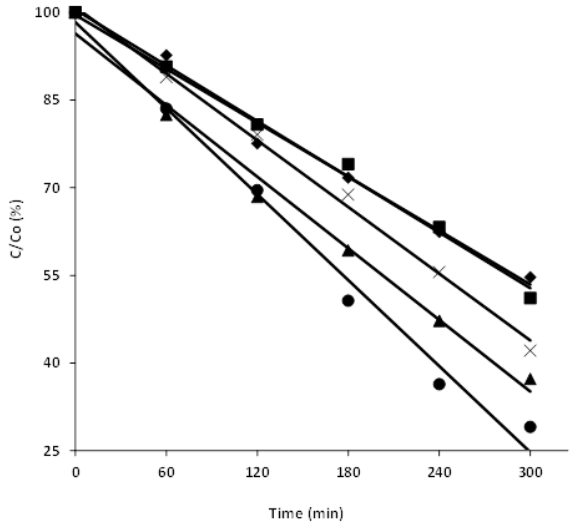

Figure 7. Photocatalytic degradation (as determined by TOC analysis) of 4-chlorophenol under visible light irradiation by P25 TiO_2 (□), C-TiO_2 with nominal 4 % C loading 1 h calcination (●), 3 h calcination (▲), 1 % W-TiO_2 (■),co-doped C, W-TiO_2 with 1% W loading and nominal 4 % C loading (X).

Degussa P25 TiO_2 also performed reasonably well in these measurements degrading 56 % of chlorophenol in 300 min (despite the fact that the experiments took place in the presence of visible light only). The UV filter film used cuts off light <410 nm and from Figure 4 it is clear that P25 TiO_2 can absorb relatively small amounts of light (generating electron hole pairs) above this wavelength. The observed activity confirms the well-known photocatalytic activity of P25 due to the high crystallinity and the inherent optimal anatase:rutile ratio existing in this grade of TiO_2.

Furthermore, even though neither TiO_2 nor Chlorophenol (CP) absorb visible light it has been reported that the TiO_2-CP_{ads} system has charge transfer bands that can absorb such radiation [54-57]. Kim and Choi have shown that charge carriers can be generated from the excitation of these charge transfer states and that there remains the possibility for a variety of photochemistries to result from reaction of these charge carriers. Gray *et al.* [55, 56] have demonstrated visible light activity for the reaction of a range of chlorophenols following excitation of these charge transfer bands. These authors have also pointed out that full mineralisation of the adsorbed species requires UV light (since the CT complex is destroyed by the first electron transfer step) but that the initial degradation (involving Cl^- formation) can proceed using visible light. Of course this process would also operate in the doped catalysts. It is then evident that the initial intermediate oxidation product can undergo further solution-based homogeneous reactions involving free radicals.

As predicted by theoretical calculations [35] and as shown by UV-vis spectroscopy here (see Figure 4 (c)), the C, W co-doped material had an absorbance significantly shifted towards the visible region. However, despite the enhanced optical properties of the W-doped and co-doped TiO_2 catalysts, these were considerably poorer photo-oxidation catalysts (see Figure 4(c)) compared to C-TiO_2 materials. This may be due to W cations acting as electron hole recombination centres due to the introduction of isolated localized d states below the conduction band [58-60].

Recently, co-doping of TiO_2 has been reported to passivate localised defect bands that may be present in mono-doped TiO_2 such that they no longer act as recombination centres [61]. Co-doping carbon and tungsten has been reported to yield such a passivation effect in comparison to singly doped tungsten or carbon TiO_2. This reported passivation is due to the formation of a C 2p - W 5d hybridized band [35] when dopants are located near one other (as the nearest neighbour or the second nearest neighbour). This strengthens hybridization between C 2p and O 2p resulting in a fully occupied band of higher energy than the top of the valence band edge and at the same time forms a continuum-like band between the conduction band and tungsten dopant d states below. This should result in enhanced photocatalytic activity in co-doped (as compared to singly doped) materials due to improved charge carrier mobility and reduced electron hole recombination. There may be some evidence of passivation of this effect by the carbon as the co-doped C,W-TiO_2 performs better than singly doped W-TiO_2. However, the activity of the co-doped sample is still lower than that of singly doped C-TiO_2.

This discrepancy between the predicted and observed behaviour may simply be due the locations of the dopants situated further from one other in the lattice and the presence of relatively low levels of carbon dopant (it was also reported that when the carbon and tungsten dopants are far from each other in the lattice the passivation effect should no longer exist [35]).

Therefore, it seems there are sufficient levels of carbon and tungsten to increase absorbance towards the visible region but insufficient carbon located near the tungsten dopant to passivate

recombination effects due to tungsten incorporation. Overall this results in a net decreased photocatalytic activity.

This result confirms that the performance of a material as a solar photocatalyst is not a function of solely the ability of the material to absorb light in the visible region of the spectrum. Other factors are also important such as the crystallinity and particle size of the material and the ability of the material to retard the electron-hole recombination process [50-53,58-60].

Many reported photocatalytic studies have repeatedly shown that the enhanced visible light absorption observed in the UV-vis spectra of catalysts does not translate into increased visible light induced photocatalytic activity. This, in fact, has stagnated this field of research for more than a decade. Most reported studies, involving doped TiO_2 photocatalysts, propose that the observed red-shift in light absorption is caused by a narrowing of the band gap of pristine TiO_2 or due to the appearance of intragap localized states of the dopants, without considering the possibility of forming colour centres that absorb in the visible light spectral region, as recently shown by Kuznetsov and Serpone [25, 62]. In the present study, the XPS data shows clearly that doping definitely occurs in the TiO_2 lattice. This is also well reflected in the increased chlorophenol photocatalytic oxidation activity of C-TiO_2 noted under visible light irradiation. On the other hand, such beneficial effects are totally absent with the W and C, W co-doped TiO_2, despite the noticeable redshifts observed in their absorption spectra. The beneficial effect of C-doped samples under solely visible irradiation cannot be the result of any inadvertant UV photon entry into the system as such a process would also have improved the activity of the W and W

and C co-doped samples. Also, the theoretically predicted advantage for photocatalysis [35] was not evident with these doped samples despite the effect of doping clearly being seen in the XPS spectra. These aspects need to be clarified for photocatalysis to be properly understood.

Based on our results, it is logical to conclude that a significant fraction of the spectral red-shift commonly observed with doped catalysts might be due to formation of colour centres as a result of defects associated with oxygen vacancies. However, even though bandgap related narrowing or intragap localization of dopant levels are possible; it seems these are not the major factors responsible for enhanced visible light absorption as commonly reported in this field of research. This also throws light onto the insensitivity of the calculated bandgap values reported in Table 1 (based on spectral absorption thresholds) to the degree of dopant concentration for the various catalysts studied here.

Photocatalytic activity experiments were also carried out under the 'full Sun' conditions (*i.e.* in the absence of a UV filter where the reaction vessels were exposed to the full AM1.5G spectrum). Again the photocatalytic degradation of 4-chlorophenol in the presence of the photocatalysts was investigated using TOC measurements.

Figure 8 shows the degradation versus time profiles for the photocatalytic oxidation of chlorophenol (determined using TOC analysis) under UV plus visible light. All the materials studied were more active under the "full Sun" conditions than they were under the "visible light

only" conditions (see figure 7), reflecting the increased number of electron hole pairs that can be generated when UV light is available to cause excitation. The order of catalytic activity however differs. Under these conditions P25 TiO_2 degrades all of the chlorophenol within two hours. C-TiO_2 (calcined for 1 hr) while the most active powder in the visible-light experiments (see Figure 7), takes over four hours to complete the total breakdown of the same levels of chlorophenol.

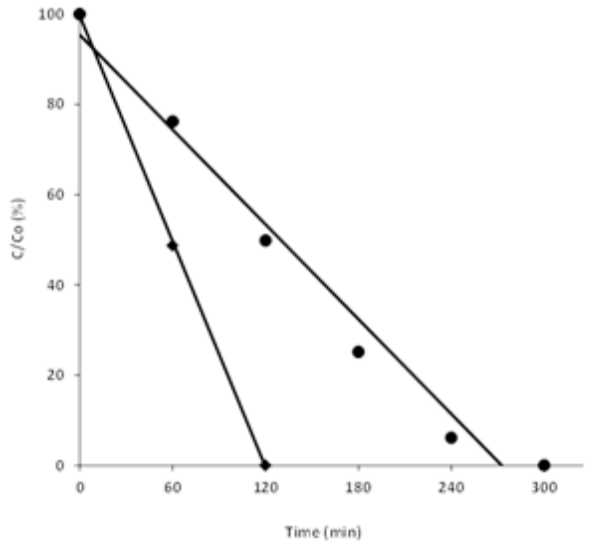

Figure 8. Photocatalytic degradation (as determined by TOC analysis) of 4-chlorophenol under UV plus visible light irradiation by P25 TiO_2 (●), C-TiO_2 with nominal 4 % C loading 1 h calcination (□).

Over TiO_2, following illumination with the appropriate energies of light and generation and separation of electron hole pairs, degradation of organic species can take place by several different pathways;

(i) directly, where the holes accept an electron from an adsorbed species. These holes can exist in the valance band of TiO_2 or in higher energy orbitals related to the presence of dopant,

$$4\text{-}CP_{(ads)} + h^+ \rightarrow 4\text{-}CP^{+\cdot}$$

(ii) indirectly via $OH^{\cdot}$ radical reactions where the radicals are formed from O_2^- species which are generated from the reduction of dissolved O_2 using the promoted electron [63] (as in the reactions shown below).

$$O_{2\ (ads)} + e^- \rightarrow O_2^-{}_{(ads)}$$

$$O_2^-{}_{(ads)} + H^+ \Leftrightarrow HO_{2\ (ads)}$$

$$HO_{2\ (ads)} + e\text{-} \rightarrow HO_2^-{}_{(ads)}$$

$$HO_2^-{}_{(ads)} + H^+ \rightarrow H_2O_{2(ads)}$$

$$H_2O_2 \Leftrightarrow 2OH^{\cdot}$$

$$2HO_2 \rightarrow H_2O_{2\ (ads)} + O_2$$

$$OH^{\cdot} + H_2O_2 \rightarrow H_2O + HO_2^{\cdot}$$

$$HO_2^{\cdot} + H_2O_2 \rightarrow H_2O + OH^{\cdot} + O_2$$

(iii) Indirectly via the generation of $OH^{\cdot}$ radicals from the oxidation of OH^- on valance band or dopant level holes.

$$OH^- + h^+ \rightarrow OH^{\cdot}$$

Under full sun conditions the un-doped TiO_2 performs better than our carbon doped TiO_2 materials despite more photons being available for electron promotion (and reaction initiation) in the latter catalyst. This indicates that the holes formed in the VB of un-doped TiO_2 are more active than those generated in the dopant related orbitals and it can be assumed that this in turn relates to the greater driving force (due to the differences in their respective redox levels) involved in neutralizing the VB holes.

Another possible reason for the lower activity of the doped materials may relate to the relative energetics of the holes formed in dopant related energy levels and the required potential for the formation of OH radicals from hydroxide anions. If these holes arise in the mid gap state in the doped TiO_2 they may exist at oxidation potentials higher than that of the OH radical formation potential ($OH^-/OH^{\cdot}$ = 1.9 V NHE). If the holes are not energetic enough to extract electrons from OH^- then the generation of these OH radicals will be retarded and one route for 4-CP degradation will be restricted. In an example of this Park et al. [18] have reported that, following carbon doping, the mid gap level lies somewhere between 1.9 and 1.4 V since they note this effect in the oxidation of 4-CP (1.9 V) with C-doped samples but less of an effect in I^- oxidation (where a potential of only 1.4 V is required).

In carbon doped TiO_2 if the mid gap energy state induced by doping lies at a higher oxidation potential than the OH radical formation potential, then the doped material, despite being able to absorb more photons, will not form OH radicals and promote indirect degradation of the 4-CP. These holes will however still degrade 4-CP via direct oxidation as the 4-CP oxidation potential (0.8 V versus NHE) still lies above the mid gap state.

Any advantage derived from being doped (and thus being able to absorb more photons of lesser energy to promote an electron) is negated by the positioning of the mid gap energy state in relation the OH radical formation potential and in effect the reaction proceeds mostly via interactions involving O_2^- which is generated in the reductive half reactions.

In our situation this route is not expected to wield a considerable effect on reactivity since the photocatalytic reactions initially have a pH of 6 (from 4-chlorophenol) and this will fall as mineralisation progresses (due to the release of HCl). This would result in low concentrations of free OH^- and a low rate of OH radical formation from OH^- oxidation.

There is now a general agreement that N-doping need not result in a shift of the VB edge (*i.e.* a shift in the O 2p states), create more or less localized N 2p states whose energies are located within the bandgap. Our results with C-doped catalysts also indicate that the doped sites, despite improving the visible light absorption characteristics, are not directly involved in the phocatalytic decomposition of surface adsorbed organics, and most of the resulting

photocatalysis occurs through O_2^- related solution reactions. [64-69]

Another critical point is that typically C doping leads to extremely low concentrations of C in the structure. We cannot assume that this concentration is sufficient to raise the bulk valence-band level by >0.5 eV and it is more likely that we are simply adding discrete energy levels at energies somewhat above the upper edge of the valance band. If this is the case, and holes generated within these energy levels are not suitable for the production of hydroxyl radicals from hydroxide ions then one major route towards organic degradation is adversely affected.

In any case, it should be noted that in practical applications of photocatalysis, light irradiation is often used to produce only the initial molecular breakdown to biodegradable fragments and the subsequent total mineralisations are often carried out by relatively less expensive biological processes. This study shows that visible light active C-doped photocatalysts prepared through the melamine borate method can perform the initial molecular fragmentation of pollutants (30 % TOC removal in 120 minutes and even up to 71% TOC removal in 300 minutes) using relatively cheaper and more energy efficient visible lamps, such as LEDs (with lifetimes of 10,000 hours), which require very low running costs. Furthermore, their use in gas phase depollution of odour causing vapours in indoor conditions is a clear possibility [70].

4. CONCLUSIONS

Carbon doped TiO_2 photocatalysts were reproducibly formed using an inexpensive and facile altered sol-gel preparation method with melamine borate as an external source of carbon dopant. The materials (which did not contain either N or B dopants) have been shown by XPS to contain carbon substitutionally doped into the TiO_2 lattice. The carbon doped TiO_2 has shown improved optical absorbance and photocatalytic activity under visible light compared to un-doped TiO_2 and Degussa P25. Carbon and tungsten co-doped materials have also been formed using this novel carbon doping approach combined with a well-known tungsten doping method [16].

The addition of tungsten improved the optical absorbance properties of the materials in accordance with reported theoretical calculations, but did not enhance their photocatalytic activity as expected from the theoretical models. This is thought to be mainly due to the effects of recombination of electron-hole pairs at the tungsten metal ion centers. A significant faction of the enhanced red-shifted light absorption is also thought to arise from colour centers associated with oxygen defects in the doped TiO_2 lattice. For further progress in visible light induced photocatalysis to be made, it will be necessary to understand the individual contributions towards spectral red-shifts arising from bandgap alterations and the formation of oxygen defect based colour centres respectively.

The activity under whole sun conditions of the materials (while being higher than the activity in visible light only conditions) is lower than that of P25 suggesting a greater driving force for neutralisation of VB holes than for neutralisation of dopant level holes. Furthermore, the holes

formed following absorbance of lower energy photons are in localised energy levels within the bandgap and these energies are not sufficient to generate active hydroxyl species. It would not be expected that this constitutes a significant route of reaction.

ACKNOWLEDGMENT

We acknowledge and thank Science Foundation Ireland for their funding of this Strategic Research Cluster Programme (07/SRC/B1160) and our Industry Partners for their support of this Cluster. We specifically thank SSE Renewables for their support of E.M.N.

SUPPORTING INFORMATION AVAILABLE

Profiles showing the W4d, W4f, N1s and B1s regions of the XPS spectra as well as a set of EPR spectra of TiO_2, C-TiO_2 and C-W-TiO_2 are in the supporting information section. This information is available free of charge via the Internet at http://pubs.acs.org.

ABBREVIATIONS

C-TiO_2, carbon doped TiO_2; W-TiO_2, tungsten doped TiO_2; C,W-TiO_2, carbon and tungsten co-doped TiO_2; VB, valence band; CB, conduction band; CP, chlorophenol; CT, charge transfer, TGA, Thermogravimetric analysis; MS, mass spectrometry, XRD, X-Ray diffraction; XPS, X-ray photoelectron spectroscopy; DRS, diffuse reflectance spectroscopy; TOC, total organic carbon.

REFERENCES

[1] Hoffmann, M.R.; Martin, S.T.; Choi, W.Y.; Bahnemann, D.W. *Chem. Rev.* **1995**, 95, 69-96

[2] Mills, A.; LeHunte, S. *J. Photochem. Photobiol. A* **1997**, 108, 1-35

[3] Ashokkumar, M. *Int. J. Hydrogen Energy* **1998**, 23, 427-438

[4] Ni, M.; Leung, M.K.H; Leung, D.Y.C.; Sumathy, K. *Renew. Sust. Energ. Rev* **2007**, 11 401-425

[5] Herrmann, J.M. *Catal. Today* **1999**, 53, 115-129

[6] Patsoura, A.; Kondarides, D.I.; Verykios, X.E. *Catal. Today* **2007**, 124, 94-102

[7] Bowker, M.; James, D.; Stone, P.; Bennett, R.; Perkins, N.; Millard, L.; Greaves, J.; Dickinson, A. *J. Catal.* **2003**, 217, 427-433

[8] Kondarides, D.I.; Daskalaki, V.M.; Patsoura, A.; Verykios, X.E. *Catal. Lett.* **2008**, 122, 26-32

[9] Bard, A.J. *J. Photochem.* **1979**, 10, 59-75

[10] Grimes, C.A.; Varghese, O.K.; Ranjan, S. *Light, Water, Hydrogen: The Solar Generation of Hydrogen by Water Photoelectrolysis*, Springer, 2008.

[11] Asahi, R.; Morikawa, T.; Ohwaki, T.; Aoki, K.; Taga, Y. *Science* **2001**, 293, 269-271

[12] Chen, D.M.; Jiang, Z.Y.; Geng, J.Q.; Wang, Q.; Yang, D. *Ind. Eng. Chem. Res.* **2007**, 46, 2741-2746

[13] Choi, W.Y.; Termin, A.; Hoffmann, M.R.; *Angew. Chem. Int. Ed*. **1994**, 33, 1091-1092

[14] Irie, H.; Watanabe, Y.; Hashimoto, K. *J. Phys. Chem. B* **2003**, 107, 5483-5486

[15] Khan, S.U.M.; Al-Shahry, M.; Ingler, W.B. *Science* **2002**, 297, 2243-2245

[16] Lorret, O.; Francova, D.; Waldner, G.; Stelzer, N. *Appl. Catal. B* **2009**, 91, 39-46

[17] Nakamura, R.; Tanaka, T.; Nakato, Y. *J. Phys. Chem. B* **2004**, 108, 10617-10620

[18] Park, Y.; Kim, W.; Park, H.; Tachikawa, T.; Majima, T.; Choi, W. *Appl. Catal. B* **2009**, 91, 355-361

[19] Sakthivel, S.; Janczarek, M.; Kisch, H. *J. Phys. Chem. B* **2004**, 108, 19384-19387

[20] Shen, X.Z.; Guo, J.; Liu, Z.C.; Xie, S.M. *Appl. Surf. Sci.* **2008**, 254, 4726-4731

[21] Tachikawa, T.; Tojo, S.; Kawai, K.; Endo, M.; Fujitsuka, M.; Ohno, T.; Nishijima, K.; Miyamoto, Z.; Majima, T. *J. Phys. Chem. B* **2004**, 108, 19299-19306

[22] Wang, C.Y.; Bahnemann, D.W.; Dohrmann, J.K. *Chem. Commun.* **2000**, 16, 1539-1540

[23] Yang, X.X.; Cao, C.D.; Erickson, L.; Hohn, K.; Maghirang, R.; Klabunde, K. *J. Catal.* **2008**, 260, 128-133

[24] Zaleska, A. *Recent Patents on Engineering* **2008**, 2, 157-164

[25] Serpone, N. *J. Phys. Chem. B* **2006**, 110, 24287-24293

[26] Sakatani, Y.; Ando, H.; Okusako, K.; Koike, H.; Nunoshige, J.; Takata, T.; Kondo, J.N.; Hara, M.; Domen, K. *J. Mater. Res.* **2004**, 19, 2100-2108

[27] Shen, Y.F.; Xiong, T.Y.; Li, T.F.; Yang, K. *Appl. Catal. B* **2008**, 83, 177-185

[28] Wang, D.; Zou, Y.H.; Wen, S.C.; Fan, D.Y. *Appl. Phys. Lett.* **2009**, 95, 012106

[29] Andersson, S.; Collen, B.; Kuylenstierna, U.; Magnéli, A. *Acta Chem. Scand.* **1957**, 11, 1641-1652

[30] Reyes-Coronado, D.; Rodriguez-Gattorno, G.; Espinosa-Pesqueira, M.E.; Cab, C.; de Coss, R.; Oskam, G. *Nanotechnology* **2008**, 19, 145605

[31] Jobbagy, M.; Couselo, N.; Einschlag, F.S.G.; Candal, R.J. *J. Phys. Chem. C* **2008**, 112, 1094-1100

[32] Yang, Y.; Wang, H.; Li, X.; Wang, C. *Mater. Lett.* **2009**, 63, 331-333

[33] Patterson, A.L. *Phys. Rev.* **1939**, 56, 978–982

[34] Sakthivel, S.; Kisch, H. *Angew. Chem. Int. Ed.* **2003**, 42, 4908-4911

[35] Long, R.; English, N.J. *Chem. Mater.* **2010**, 22, 1616-1623

[36] Sun, H.Q.; Bai, Y.; Cheng, Y.P.; Jin, W.Q.; Xu, N.P. *Ind. Eng. Chem. Res.* **2006**, 45, 4971-4976

[37] Papirer, E.; Lacroix, R.; Donnet, J.B.; Nanse, G.; Fioux, P. *Carbon* **1995**, 33, 63-72

[38] Li, Y.Z.; Hwang, D.S.; Lee, N.H.; Kim, S.J. *Chem. Phys. Lett.* **2005**, 404, 25-29

[39] Ohno, T.; Tsubota, T.; Nishijima, K.; Miyamoto, Z. *Chem. Lett.* **2004**, 33, 750-751

[40] Ren, W.J., Ai, Z.H.; Jia, F.L.; Zhang, L.Z.; Fan, X.X.; Zou, Z.G. *Appl. Catal. B* **2007**, 69, 138-144

[41] In, S.I.; Kean, A.H.; Orlov, A.; Tikhov, M.S.; Lambert, R.M. *Energ. Environ. Science* **2009**, 2, 1277-1279

[42] Irie, H.; Washizuka, S.; Hashimoto K., *Thin Solid Films* **2006**, 510, 21-25

[43] Irie, H.; Watanabe, Y.; Hashimoto, K. *Chem. Lett.* **2003**, 32, 772-773

[44] Hsu, S.W.; Yang, T.S.; Chen, T.K.; Wong, M.S. *Thin Solid Films* **2007**, 515, 3521-3526

[45] Li, X.Z.; Li, F.B.; Yang, C.L.; Ge, W.K. *J. Photochem. Photobiol. A* **2001**, 141, 209-217

[46] D. Mitoraj and H. Kisch, *Angew. Chem. Int. Ed.* **2008**, 47, 9975-9978

[47] Dhananjeyan, M.R.; Kiwi, J.; Thampi, K.R. *Chem. Commun.* **2000** 1443-1444

[48] Dhananjeyan, M.R.; Mielczarski, E.; Thampi, K.R.; Buffat, P.; Bensimon, M.; Kulik, A.; Mielczarski, J.; Kiwi, J. *J. Phys. Chem. B* **2001**, 105, 12046-12055

[49] Ohtani, B.; Ogawa, Y.; Nishimoto, S. *J. Phys. Chem. B* **1997**, 101, 3746-3752

[50] Binitha, N.N.; Yaakob, Z.; Resmi, R. *Cent. Eur. J. Chem.* **2010**, 8, 182-187

[51] Anpo, M.; Aikawa, N.; Kodama, S.; Kubokawa, Y. *J. Phys. Chem.* **1987**, 91, 4305-4310

[52] Ho, W.K.; Yu, J.C.; Lee, S.C. *J. Solid State Chem.* **2006**, 179, 1171-1176

[53] Bickley, R.I.; Gonzalezcarreno, T.; Lees, J.S.; Palmisano, L.; Tilley, R.J.D. *J. Solid State Chem.* **1991**, 92, 178-190

[54] Kim, S.; Choi, W. *J. Phys. Chem. B* **2005**, 109, 5143-5149

[55] Hurum, D.C.; Gray, K.A.; Rajh, T.; Thurnauer, M.C. *J. Phys. Chem. B* **2004**, 108, 16483-16487

[56] Agrios, A.G.; Gray, K.A.; Weitz, E. *Langmuir* **2003**, 19, 1402-1409

[57] Usseglio, S.; Calza, P.; Damin, A.; Minero, C.; Bordiga, S.; Lamberti, C.; Pelizzetti, E.; Zecchina, A. *Chem. Mater.* **2006**, 18, 3412-3424

[58] Herrmann, J.M.; Disdier, J.; Pichat, P. *Chem. Phys. Lett.* **1984**, 108, 618-622

[59] Lou, Z.; Gao, Q. *Photochem. Photobiol. A* **1992**, 63, 367-375

[60] Umebayashi, T.; Yamaki, T.; Itoh, H.; Asai, K. *J. Phys. Chem. Solids* **2002**, 63, 1909-1920

[61] Gai, Y.Q.; Li, J.B.; Li, S.S.; Xia, J.B.; Wei, S.H. *Phys. Rev. Lett.* **2009**, 102, 036402

[62] Kuznetsov, V.N.; Serpone, N.J. *J. Phys. Chem. B*, **2006**, 110, 25203–25209

[63] Vinodgopal, K.; Stafford, U.; Gray, K.A.; Kamat, P.V. *J. Phys. Chem.* **1994**, 98, 6797-6803

[64] Nah, Y-C.; Paramasivam, I.; Schmuki, P. *ChemPhysChem*, **2010**, 11, 2698 – 2713

[65] Henderson, M.A. *Surf. Sci. Rep.* **2011**, 66 185–297

[66] Di Valentin, C.; Pacchioni, G.; Selloni, A.; Livraghi, S.; Giamello, E. *J. Phys. Chem. B* **2005**, 109, 11414-11419

[67] Di Valentin, C.; Finazzi, E.; Pacchioni, G.; Selloni, A.; Livraghi, S.; Paganini, M.C.; Giamello, E. *Chem. Phys.* **2007**, 339, 44-56

[68] Finazzi, E.; Di Valentin, C.; Selloni, A.; Pacchioni, G. *J. Phys. Chem. C* **2007**, 111, 9275-9282

[69] Graciani, J.; Alvarez, L.J.; Rodriguez, J.A.; Sanz, J.F. *J. Phys. Chem. C* **2008**, 112, 2624-3261

[70] Kandavelu, V.; Kastien, H.; Thampi, K. R. *Appl. Catal. B* **2004**, 48, 101–111

Supporting Information

Figure S1

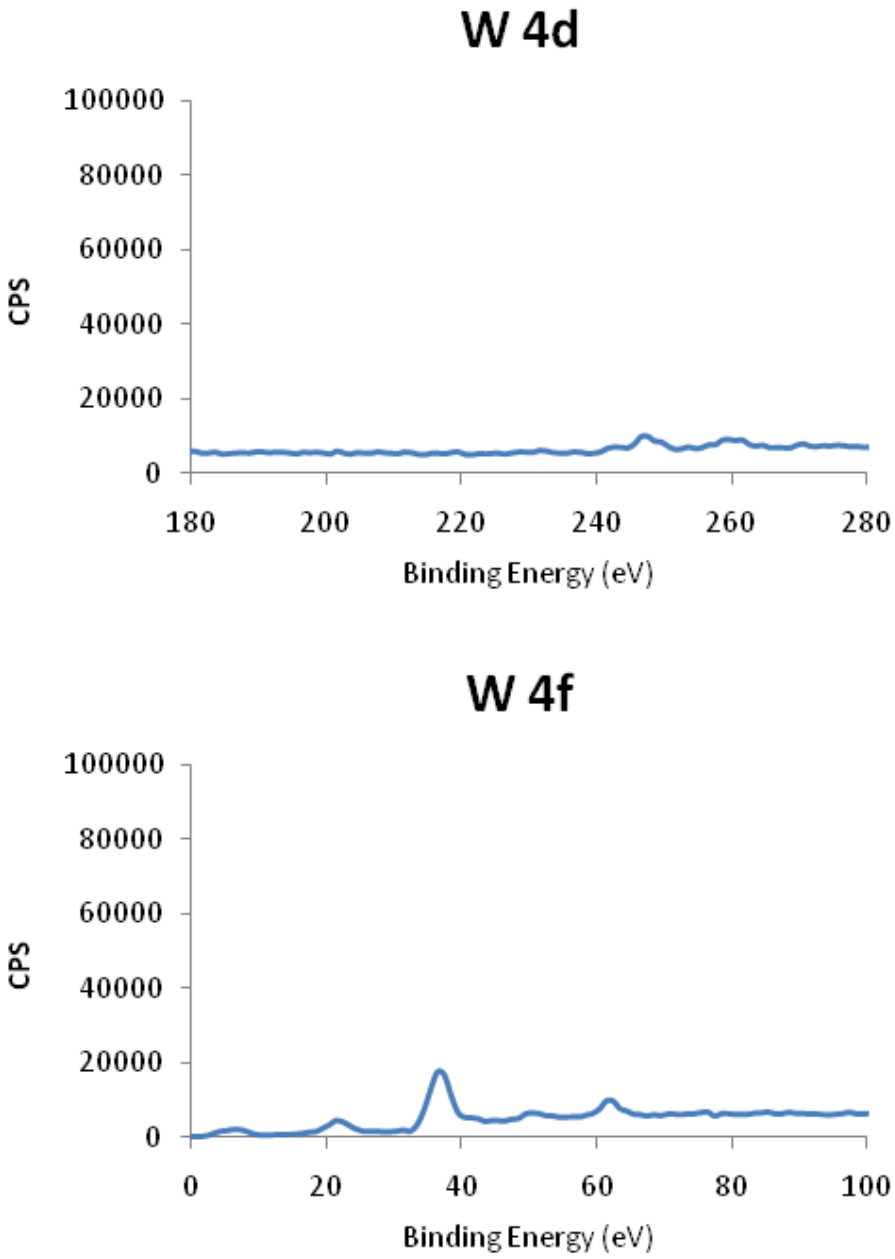

Figure S1 from W $4d_{5/2}$ and W $4d_{3/2}$ levels at 247.2 and 259.7 eV and a peak at 36.6 eV due to electron ejection from the W 4f level

Figure S2

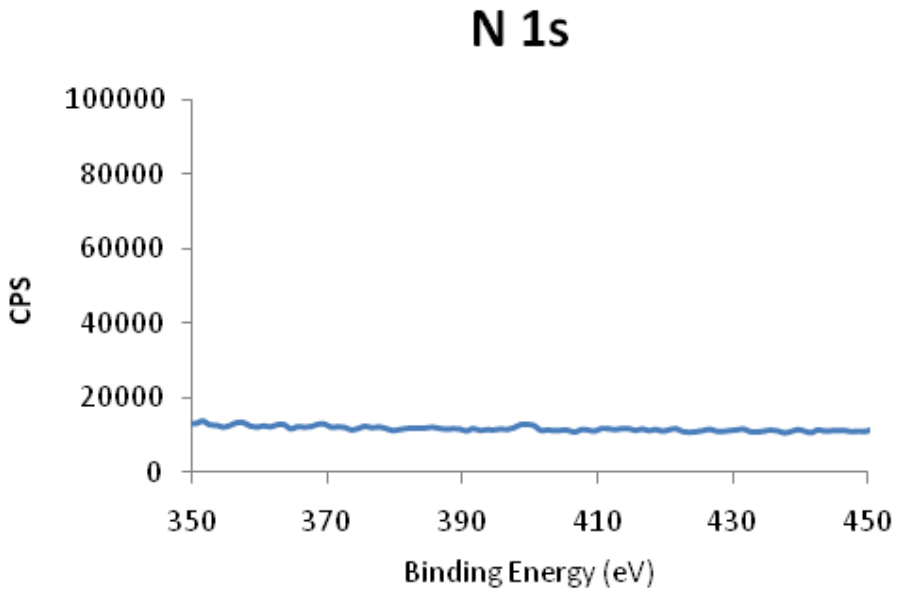

Figure S2 XPS profile of a typical doped material (nominally 4% C doped TiO_2) showing the N 1s region of the spectrum (peaks would be expected between 399 and 401 eV)

Figure S3

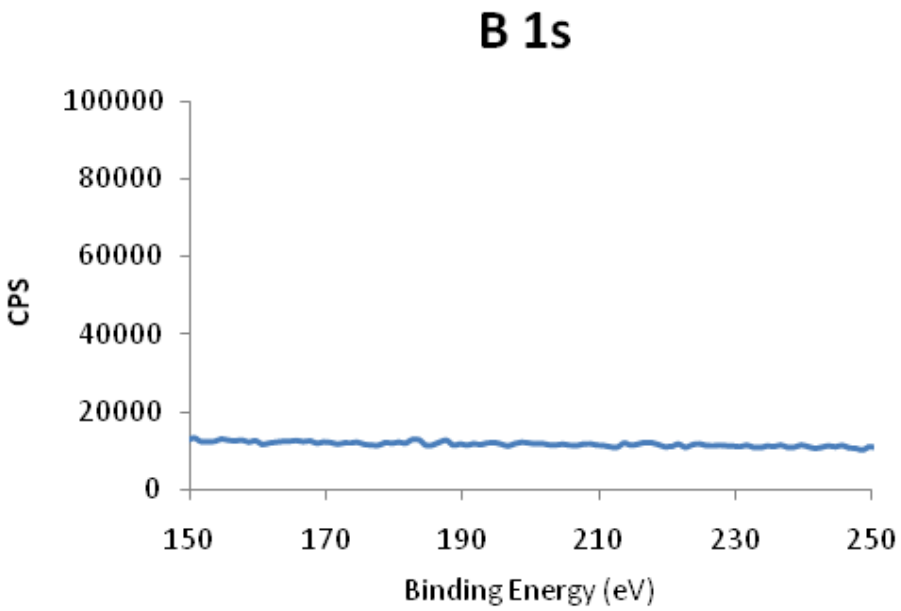

Figure S3 XPS profile of a typical doped material (nominally C doped TiO_2) showing the B 1s region of the spectrum (peaks would be expected between 185 and 192 eV).